(Received 24 January 2025, Accepted 12 March 2025, Scheduled 20 March 2025)

A Circularly Polarized Magnetoelectric Dipole Antenna with Microstrip-Line Aperture-Coupled Feeding

Wusheng Ji[1, 2, *], Yun Gao[1, 2], Xingyong Jiang[3], Xinyi Li[1, 2], and Wenhan Wan[1, 2]

[1] *Institute of Antenna and Microwave Techniques, Tianjin University of Technology and Education, Tianjin 300222, China*
[2] *School of Electronic Engineering, Tianjin University of Technology and Education, Tianjin 300222, China*
[3] *Rofs Microsystem, Tianjin 300462, China*

ABSTRACT: This paper presents a high-gain right-hand circularly polarized (RHCP) magnetoelectric (ME) dipole antenna (MEDA) with microstrip-line aperture-coupled feeding. By extending one pair of diagonal horizontal metallic plates in the traditional linearly polarized MEDA in opposite directions, the electric dipole current becomes parallel to the magnetic dipole current, achieving circular polarization performance. The antenna is excited using a microstrip-line aperture-coupled feeding structure, and its electrical performance is further enhanced by integrating a box-shaped reflector. The measured results of the antenna prototype show that the impedance bandwidth ($|S_{11}| \leq -10$ dB) is 46.8% (2.90–4.67 GHz); the 3 dB axial ratio bandwidth is 26.4% (3.58–4.67 GHz); and the maximum in-band gain reaches 12.9 dBic. A cross-polarization level below -18 dB and a front-to-back ratio exceeding 20 dB highlight the superior performance of the proposed antenna.

1. INTRODUCTION

With the rapid development of modern wireless communication systems, achieving more stable communication under complex environments and conditions has become increasingly critical. Circularly polarized (CP) antennas are widely employed in applications such as satellite communication, aeronautical communication, and deep-space exploration due to their high adaptability to signal propagation, resistance to multipath effects, and robustness against polarization interference. Extensive research has been conducted on circularly polarized patch antennas [1, 2], circularly polarized dielectric resonator antennas [3, 4], and helical antennas [5–7].

In 2006, Luk and Wong proposed a MEDA based on the complementary principle [8]. The MEDA features a wide impedance bandwidth, stable and symmetric radiation patterns, low back-lobe radiation, and low cross-polarization, making it an ideal choice for wireless communication systems. In 2009, Mak and Luk introduced a circularly polarized (CP) magnetoelectric dipole antenna [9], composed of two bowtie patch antennas and two trapezoidal electric dipoles. Circular polarization was achieved by connecting the two antenna ports using a power divider with a 90° phase difference. Subsequent studies have focused on low-profile designs for CP MEDAs. In [10], a low-profile design was achieved by incorporating curved slots into the vertical patch, reducing the antenna height to $0.11\lambda_0$. In [11], vertical metallic walls were replaced with embedded metallic vias in the substrate, further lowering the antenna profile to $0.05\lambda_0$. Wideband performance enhancement has been a critical topic in antenna design [12–14]. In [14], a pair of symmetrically rotated horizontal patches served as electric dipoles, while two vertical patches functioned as magnetic dipoles, achieving wide bandwidth and excellent radiation performance. Significant progress has also been made in improving the gain of CPMEDAs [15–17]. In [17], rectangular blocks were etched onto a pair of long electric dipoles, while a pair of short electric dipoles were grounded to achieve broadband circular polarization. Using this CP antenna as a unit, a 4×4 circularly polarized MEDA array was designed and fabricated. This array exhibited an impedance bandwidth of 50% (24.5–40.8 GHz), a 3 dB axial ratio bandwidth of 44% (27.5–43 GHz), and a maximum gain of 19.2 dBic. The aforementioned antenna studies all utilized coaxial feeding methods to excite the antennas. However, coaxial feeding has several drawbacks: the coaxial feed structure is not conducive to efficient integration with planar circuits; the parasitic effects of external connectors and cables can lead to higher radiation losses and poor impedance matching; and the electrical contact points of the coaxial line are prone to short-circuit issues, thereby reducing system reliability.

In recent years, the use of microstrip-line aperture-coupled feeding structures to excite CPMEDAs has gained significant attention in academia [18, 19]. Ref. [18] proposed a broadband CPMEDA with a microstrip-line aperture-coupled feeding structure. This antenna achieved an impedance bandwidth (VSWR $\leq$ 2) of 65% within the range of 2.97–5.85 GHz and a 3 dB axial ratio bandwidth of approximately 75% (2.7–5.8 GHz). However, its complex feeding network increased the overall design complexity. In [19], circular polarization was realized by connecting two diagonal horizontal electric dipole plates using metallic strips, and a printed mushroom-shaped electromagnetic bandgap (EBG) surface was added beneath the microstrip line to effectively reduce back radiation

* Corresponding author: Wusheng Ji (jiwusheng@tute.edu.cn).

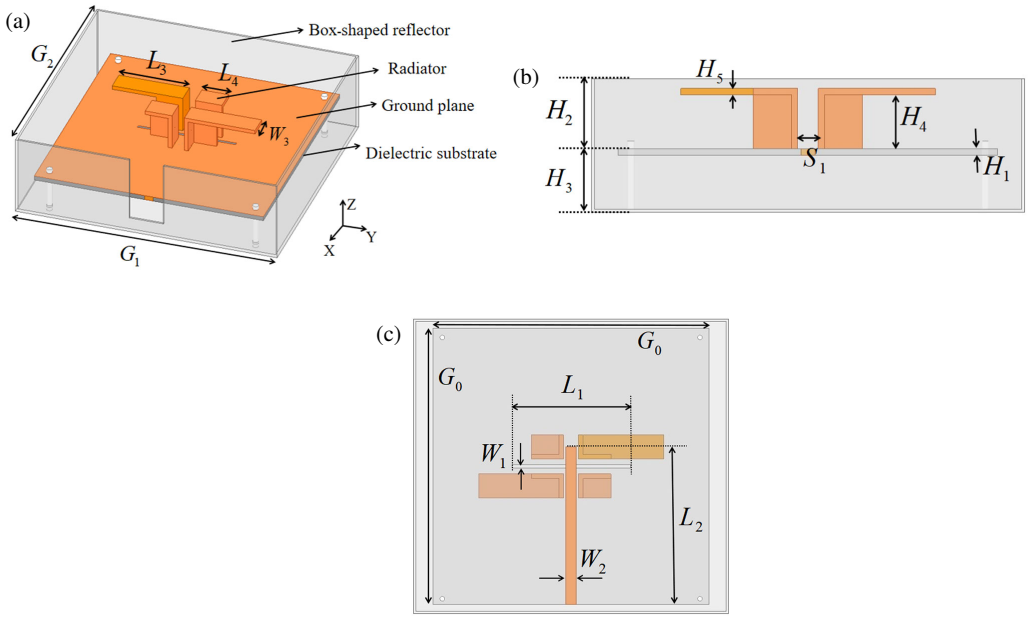

FIGURE 1. Schematic diagram of the antenna structure. (a) Three-dimensional view of the antenna; (b) Front view of the antenna; (c) Bottom view of the antenna.

caused by ground-plane apertures. However, the introduction of the EBG surface significantly increased the fabrication complexity of the antenna. Extensive studies have also been conducted on antenna array designs based on CPMEDA elements using microstrip-line aperture-coupled feeding structures [20–22]. Ref. [21], building upon the classical linearly polarized MEDA structure [23], achieved a broadband CP antenna element by introducing "L" shaped strips and adjusting the patch dimensions. An 8×8 CP antenna array was designed, featuring a total bandwidth of 31.7% (30.2–41.6 GHz) and a peak gain of 22 dBic. However, the array design reduced the radiation efficiency of the antenna, and the large overall profile of the array imposed limitations on its potential application scenarios.

This paper presents a high-gain RHCP MEDA fed by a microstrip-line aperture-coupled structure. Circular polarization is achieved by reversely extending a pair of diagonal horizontal metallic plates and exciting the antenna with the microstrip-line aperture-coupled feeding. The incorporation of a box-shaped reflector significantly enhances the antenna's gain, front-to-back ratio, and circular polarization characteristics. The proposed antenna design demonstrates high and stable gain, low cross-polarization, and minimal back radiation. Moreover, its simple structure ensures ease of fabrication and assembly.

2. ANTENNA STRUCTURE AND DESCRIPTION

The structure of the proposed CP-MEDA is shown in Figure 1. It consists of three main components: a printed dielectric substrate, a box-shaped reflector, and a CP radiator. The printed dielectric substrate is situated at the center of the antenna's overall structure. It is fabricated from a square AD450 material with a relative permittivity of 4.5 and a loss tangent of 0.0002. The substrate has a side length of G_0 and a thickness of H_1. A metallic ground plane is deposited on the upper surface of the dielectric substrate. A rectangular slot, with a length of L_1 and a width of W_1, is etched along the y-axis at the center of the ground plane. A microstrip line is etched on the lower surface of the printed dielectric substrate, which is orthogonal to the slot in the ground plane. The microstrip line has a length of L_2 and a width of W_2. The box-shaped reflector is composed of four vertical metal walls and a bottom metal plate, positioned at the base of the antenna and secured to the dielectric substrate via nylon studs. The vertical metal walls extend to a height of H_2 above the ground plane and a depth of H_3 below the ground plane. The bottom metal plate has a length of G_1 along the y-axis and a length of G_2 along the x-axis. The CP radiator is mounted on the ground plane and consists of two sets of long and short radiating elements, with a consistent spacing of S_1 between the elements. The radiating elements have a height of H_4, with the lengths of the long and short radiating elements being L_3 and L_4, respectively, and a uniform width of W_3. The detailed dimensions of the antenna are listed in Table 1.

TABLE 1. Antenna dimension parameters.

Parameters	G_0	G_1	G_2	H_1	H_2	H_3
Value (mm)	120	135	126	2	22	19
Parameters	H_4	H_5	L_1	L_2	L_3	L_4
Value (mm)	18	2	51.5	68.5	37	14
Parameters	W_1	W_2	W_3	S_1		
Value (mm)	1.5	4.5	10.5	6.5		

3. ANTENNA ANALYSIS

3.1. Antenna Design Process

The design process of the proposed CP-MEDA is shown in Figure 2. The performance of two reference antennas and

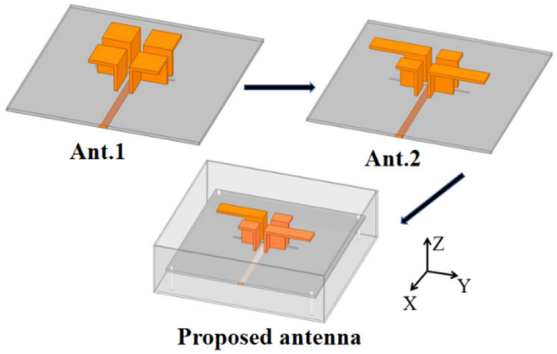

FIGURE 2. The proposed antenna and two reference antennas.

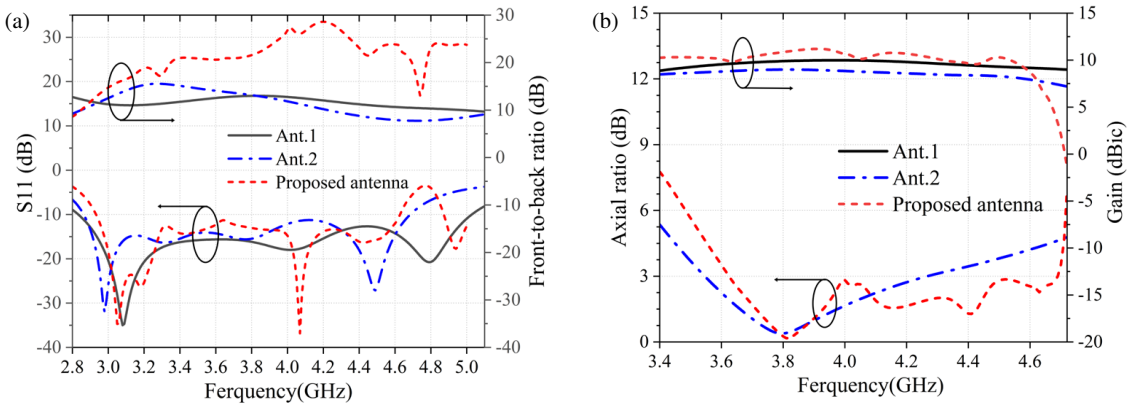

FIGURE 3. Comparison of performance between the reference antenna and proposed antenna. (a) S_{11} and front-to-back ratio; (b) Axial ratio and gain.

the proposed antenna is shown in Figure 3. Antenna 1 is a linearly polarized MEDA fed by microstrip-line aperture-coupling, with an impedance bandwidth ($|S_{11}| \leq -10$ dB) of 55.9% (2.83–5.03 GHz), a front-to-back ratio above 10 dB, and an average gain of 9.3 dBi. By adjusting the vertical metal wall and horizontal metal plates of the radiator in Antenna 1, Antenna 2 was obtained. From the axial ratio curve in Figure 3, it is evident that Antenna 2 achieves circular polarization. Its impedance bandwidth ($|S_{11}| \leq -10$ dB) is 48.3% (2.86–4.68 GHz), with a 3 dB axial ratio bandwidth of 18.5% (3.54–4.26 GHz), a maximum gain of 8.9 dBic, an average gain of 8.5 dBic, and a front-to-back ratio greater than 8 dB. Based on Antenna 2, the proposed MEDA is achieved by adding a box-shaped reflector. This antenna has an impedance bandwidth ($|S_{11}| \leq -10$ dB) of 45.0% (2.93–4.63 GHz), a 3 dB axial ratio bandwidth of 25.8% (3.62–4.69 GHz), and an overlapping bandwidth of 24.5% (3.62–4.63 GHz), with a maximum gain of 11.2 dBic and a front-to-back ratio above 20 dB within the 3 dB axial ratio bandwidth. Therefore, the addition of the box-shaped reflector has a positive impact on the antenna's front-to-back ratio, circular polarization performance, and gain. Compared with Antenna 2, the proposed antenna's front-to-back ratio is improved by more than 10 dB; the 3 dB axial ratio bandwidth is extended by 0.43 GHz; and the maximum gain is increased by 1.3 dB.

3.2. Working Principle of the Proposed Antenna

The conceptual models of the electric dipole and magnetic dipole are shown in Figure 4. The electric field expression for the radiated electric field (E-field) of the electric dipole is given by (1),

$$E_\theta \approx j\,\frac{\eta k I_0 l}{4\pi r}\,\sin\theta e^{-jkr} \tag{1}$$

where l is the length of the dipole, I_0 the current magnitude, r the radiation distance, and k the propagation wavenumber. As shown in Figure 4(b), a small loop antenna can be regarded as a magnetic dipole that is not found in nature. The radiated

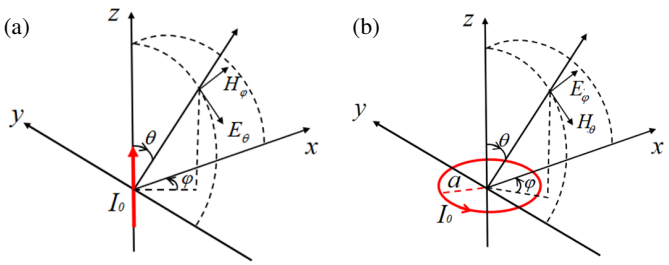

FIGURE 4. The conceptual model of the electric dipole and the equivalent magnetic dipole. (a) Electric dipole; (b) Equivalent magnetic dipole.

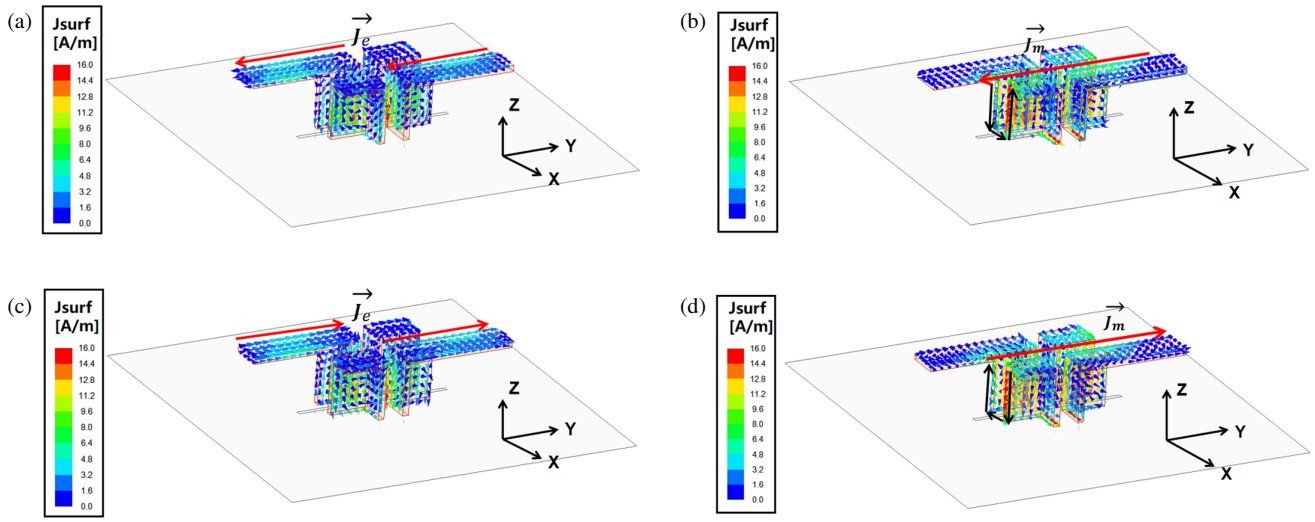

FIGURE 5. Surface current distribution of the radiator at 3.7 GHz. (a) $t = 0$; (b) $t = T/4$; (c) $t = T/2$; (d) $t = 3T/4$.

E-field of the small loop antenna can be written as

$$E_\varphi \approx \frac{\eta k^2 a^2 I_0}{4r} \sin\theta e^{-jkr} \tag{2}$$

where a is the radius of the loop antenna [21]. From (1) and (2), it can be observed that the imaginary factor j exists only in the electric field of the radiation from the electric dipole. This indicates that the fields radiated by the electric dipole and the charged circular loop under the same current excitation are orthogonal in time and phase. Therefore, if the current of the electric dipole is parallel to the magnetoelectric current generated by the loop antenna, two orthogonal electric field components in both space and time can be obtained. When the amplitudes of the electric field components are equal, a circularly polarized wave will be formed [17, 24, 25].

Figure 5 simulates the surface current distribution of the CP radiator at different time instances at 3.7 GHz. As shown in Figure 5(a), at $t = 0$, the current on the long horizontal metal plate dominates, while the current on the vertical metal walls is relatively weak. At this moment, the CP radiator operates in the electric dipole mode, with the horizontal current $\vec{J_e}$ parallel to the y-axis. As illustrated in Figure 5(b), at $t = T/4$, the current on the long metal plate gradually diminishes, and the current on the vertical metal walls becomes dominant, generating a loop current equivalent to a magnetic current $\vec{J_m}$. Consequently, the radiator operates in the magnetic dipole mode, with the equivalent magnetic current $\vec{J_m}$ parallel to the y-axis. From Figures 5(c) and 5(d), it can be observed that at $t = T/2$ and $3T/4$, the current distributions are similar to those at $t = 0$ and $t = T/4$, but the current directions are reversed. The radiator operates in the electric dipole and magnetic dipole modes, respectively. It is evident that the current on the horizontal metal plate and the magnetic current generated by the current loop on the vertical walls are parallel, and they alternate every quarter period, achieving circular polarization. Additionally, the current on the surface of the horizontal metal plate rotates counterclockwise, indicating that the antenna operates in the right-hand circularly polarized (RHCP) mode. To achieve left-hand circularly polarized (LHCP) mode, it is only necessary to swap the positions of the long and short horizontal metal plates. This simple structural adjustment can effectively alter the polarization of the antenna, thereby meeting the requirements of different application scenarios.

3.3. Key Parameter Study of the Antenna

To analyze the impact of key parameter variations on the antenna performance, detailed parameter sweeps were conducted using simulation software.

H_4 represents the height of the vertical walls of the CP radiator, and its impact on antenna performance is shown in Figure 6. From the reflection coefficient curves in Figure 6(a), it can be observed that as H_4 increases, the impedance bandwidth initially widens and then narrows. The best impedance matching is achieved when $H_4 = 19.0$ mm. According to the gain curves in Figure 6(a), the antenna gain gradually increases and becomes more stable across the operating bandwidth as H_4 increases. From the axial ratio curves in Figure 6(b), the 3 dB axial ratio bandwidth initially widens and then narrows with the increase in H_4, reaching a maximum axial ratio bandwidth of 25.8% (3.62–4.69 GHz) when $H_4 = 19.0$ mm. In summary, selecting $H_4 = 19.0$ mm ensures optimal impedance matching and circular polarization performance.

L_3 represents the length of the horizontal long metal plate of the CP radiator, and its effect on antenna performance is shown in Figure 7. From the reflection coefficient curves in Figure 7(a), it can be observed that as L_3 increases, the impedance bandwidth initially widens and then narrows, achieving the best impedance matching when $L_3 = 37$ mm. The gain curves in Figure 7(a) show that the variation in L_3 has a negligible effect on the antenna gain across the operating bandwidth. From the axial ratio curves in Figure 7(b), when $L_3 < 37$ mm, the antenna's 3 dB axial ratio bandwidth consists of two narrow passbands, and when $L_3 > 37$ mm, the axial ratio bandwidth decreases. The maximum axial ratio bandwidth of 25.8% (3.62–4.69 GHz) is achieved when $L_3 = 37$ mm. In conclusion, se-

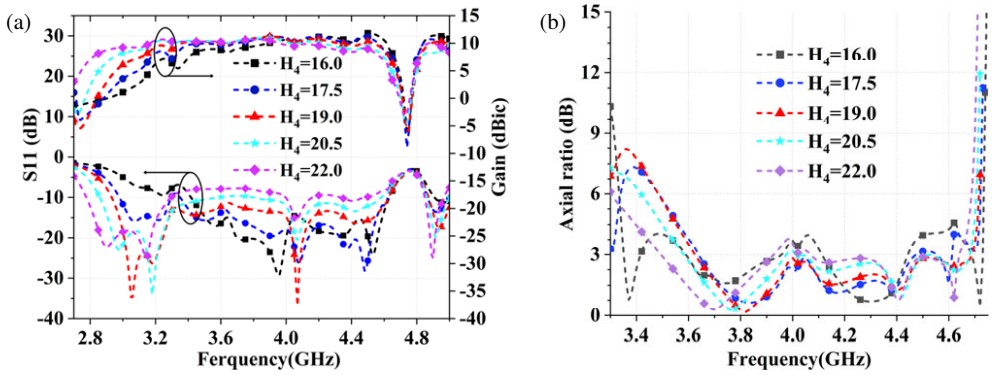

FIGURE 6. The impact of H_4 on antenna performance. (a) S_{11} and gain; (b) Axial ratio.

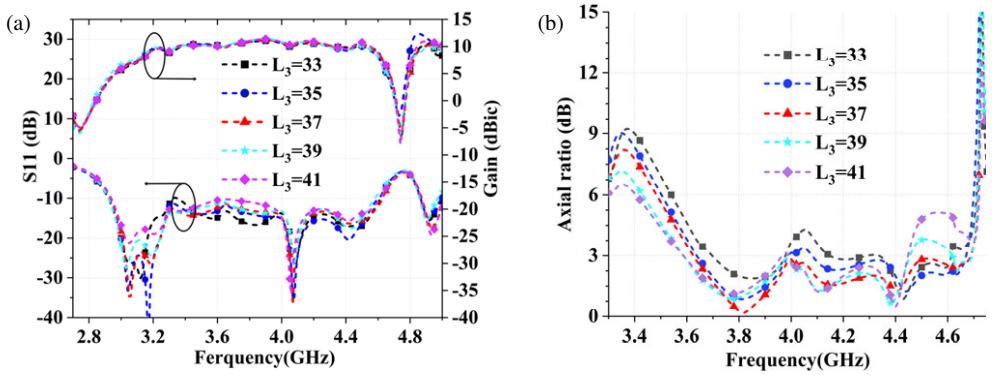

FIGURE 7. The impact of L_3 on antenna performance. (a) S_{11} and gain; (b) Axial ratio.

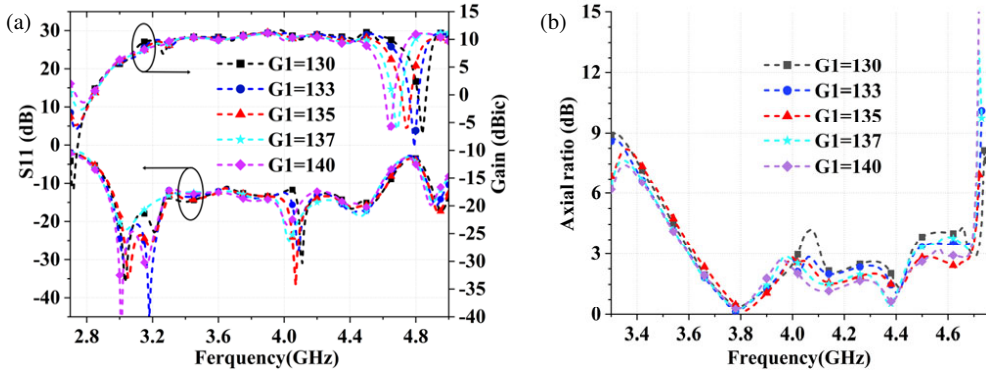

FIGURE 8. The impact of G_1 on antenna performance. (a) S_{11} and gain; (b) Axial ratio.

lecting $L_3 = 37$ mm ensures optimal impedance matching and circular polarization performance.

G_1 represents the length of the horizontal metal plate at the bottom of the box-shaped reflector along the y-axis, and its impact on antenna performance is shown in Figure 8. From the reflection coefficient curves in Figure 8(a), it can be observed that as G_1 increases, the impedance bandwidth shifts toward lower frequencies. The gain curves in Figure 8(a) indicate that within the operating bandwidth, the stable high-frequency gain of the antenna gradually decreases as G_1 increases. From the axial ratio curves in Figure 8(b), it can be seen that as G_1 increases, the 3 dB axial ratio bandwidth initially widens and then narrows, with the maximum axial ratio bandwidth of 25.8% (3.62–4.69 GHz) achieved when $G_1 = 135$ mm. In conclusion, selecting $G_1 = 135$ mm ensures stable high gain and excellent circular polarization performance.

G_2 represents the length of the horizontal metal plate at the bottom of the box-shaped reflector along the x-axis, and its impact on antenna performance is shown in Figure 9. From the reflection coefficient curves in Figure 9(a), it can be observed that as G_2 increases, the high-frequency edge of the impedance bandwidth shifts toward lower frequencies. The gain curves in Figure 9(a) indicate that within the operating bandwidth, the stable gain at higher frequencies gradually decreases as G_2 increases. From the axial ratio curves in Figure 9(b), it can be seen that as G_2 increases, the 3 dB axial ratio bandwidth ini-

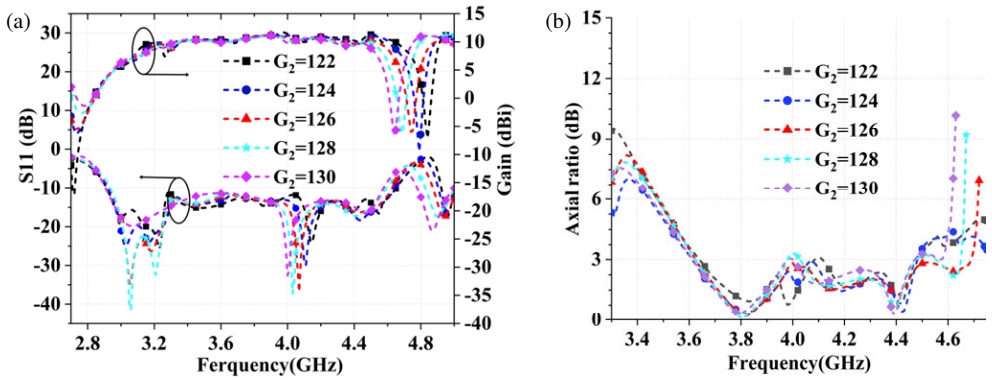

FIGURE 9. The impact of G_2 on antenna performance. (a) S_{11} and gain; (b) Axial ratio.

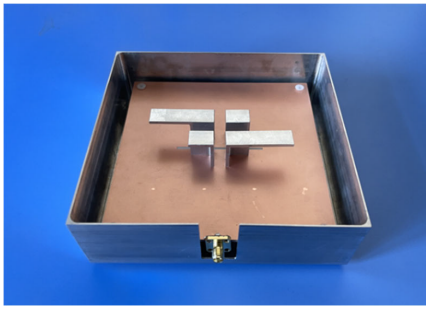

FIGURE 10. Photograph of the antenna prototype.

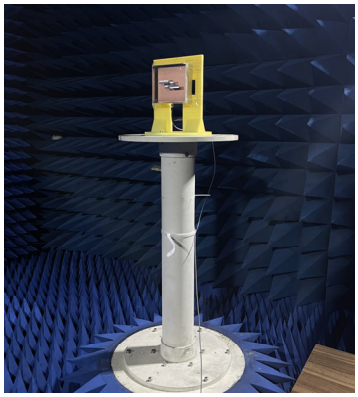

FIGURE 11. Photograph of microwave anechoic chamber measurement.

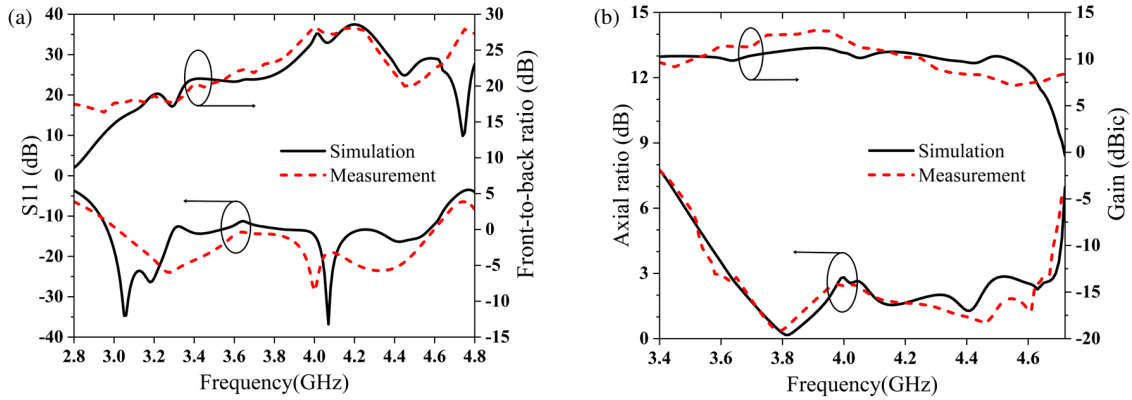

FIGURE 12. Simulation and measurement results of the antenna. (a) S_{11} and front-to-back ratio; (b) Axial ratio and gain.

tially widens and then narrows, with the maximum axial ratio bandwidth achieved when $G_2 = 126$ mm. In conclusion, selecting $G_2 = 126$ mm ensures stable gain and excellent circular polarization performance.

4. ANTENNA FABRICATION AND MEASUREMENT RESULTS

4.1. Antenna Fabrication

The proposed antenna was fabricated using mechanical processing and printed circuit board (PCB) techniques, and its performance was validated through measurements conducted in a microwave anechoic chamber. The fabricated antenna prototype is shown in Figure 10. The PCB utilizes an AD450 dielectric substrate, while the box-shaped reflector is made of aluminum plates with a thickness of 1 mm. The ME dipole radiator is constructed using 2 mm thick aluminum plates. Both the box-shaped reflector and ME dipole radiator are secured to the dielectric substrate using nylon screws, ensuring easy assembly and disassembly of the antenna components. Figure 11 shows a photograph of the proposed antenna being measured in a microwave anechoic chamber.

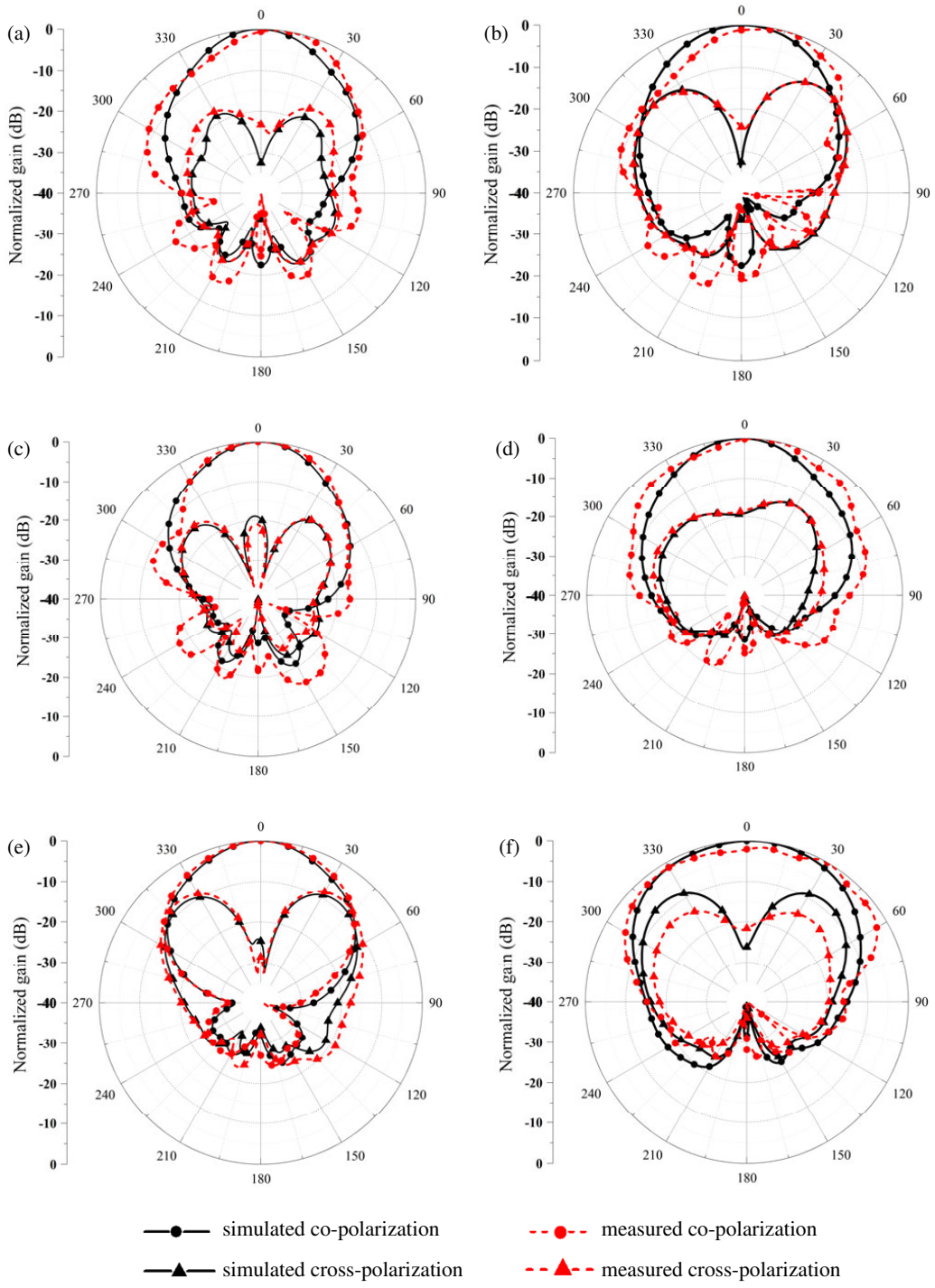

FIGURE 13. Simulated and measured radiation patterns of the antenna. (a) E-plane at 3.8 GHz; (b) H-plane at 3.8 GHz; (c) E-plane at 4.1 GHz; (d) H-plane at 4.1 GHz; (e) E-plane at 4.4 GHz; (f) H-plane at 4.4 GHz.

4.2. Antenna Measurement Results

The simulation and measurement results of the proposed CP-MEDA are shown in Figure 12. The simulated and measured impedance bandwidths ($|S_{11}| \leq -10$ dB) are 45.0% (2.93–4.63 GHz) and 46.8% (2.90–4.67 GHz), respectively. The 3 dB axial ratio bandwidths are 25.8% (3.62–4.69 GHz) and 26.4% (3.58–4.67 GHz), respectively. The simulated and measured overlapping bandwidths are 24.5% (3.62–4.63 GHz) and 26.4% (3.58–4.67 GHz), respectively. The simulated and measured maximum gains within the bandwidth are 11.2 dBic and 12.9 dBic, respectively, and the front-to-back ratio within the 3 dB axial ratio bandwidth is greater than 20 dB.

As shown in Figure 13, the simulated and measured radiation patterns of the antenna at frequencies of 3.8 GHz, 4.1 GHz, and 4.4 GHz are presented. The simulation and measurement results exhibit good agreement. At all frequencies, the E-plane and H-plane radiation patterns demonstrate good symmetry,

TABLE 2. Comparison of performance with published CP-MEDAs.

Ref.	Feeding method	Impedance bandwidth (%)	Axial ratio bandwidth (%)	Maximum gain (dBic)	Size (λ_0^3)	Manufacturing cost
[10]	Coaxial Probe	79.5	70.6	11.2	$1.46 * 1.46 * 0.11$	Moderate-cost
[14]	Coaxial Probe	65	71.5	8	$1.60 * 1.29 * 0.267$	Low-cost
[17]	Coaxial Probe	50	44	19.2	$3.28 * 3.28 * 0.167$	High-cost
[19]	aperture-coupled	58	28.4	8.9	$1.62 * 1.62 * 0.372$	Moderate-cost
[20]	aperture-coupled	18.2	16.5	26.1	$6.21 * 6.91 * 0.50$	High-cost
This work	aperture-coupled	46.8	26.4	12.9	$1.68 * 1.57 * 0.51$	Low-cost

λ_0 is the free-space wavelength at the center frequency. The definition of impedance bandwidth: [10]: $|S_{11}| < -10$ dB; [14]: VSWR < 2; [17]: $|S_{11}| < -10$ dB; [19]: VSWR < 2; [20]: $|S_{11}| < -10$ dB; This work: $|S_{11}| < -10$ dB.

consistent with the characteristics of the MEDA. At each frequency point, the simulated and measured cross-polarization levels (left-hand circular polarization) in the $+z$ direction are below -18 dB, highlighting the low cross-polarization characteristics of the antenna. Within the 3 dB axial ratio bandwidth, the simulated and measured front-to-back ratios of the antenna are greater than 20 dB, reflecting the high front-to-back ratio performance. In conclusion, the CP antenna exhibits excellent radiation characteristics.

The performance comparison between the proposed antenna and published CP-MEDAs is shown in Table 2. Ref. [10] employed a power divider and a 90° phase shifter to dual-feed a dual-polarized antenna, achieving wideband circular polarization. However, the antenna exhibited significant gain fluctuations within the operating bandwidth, leading to instability. Ref. [14] achieved wideband circular polarization by equivalently modeling a pair of rotationally symmetric curved metallic plates as electric dipoles and loading a reflector with dual slots. However, its peak gain of 8.6 dBic falls short of meeting the high-gain requirements of modern communications. In [17], a wideband CP antenna was used as a unit to design and fabricate a 4×4 CP-MEDA array, achieving excellent wideband and high-gain performance. However, the array design increased the complexity of the antenna fabrication process and reduced its radiation efficiency. Ref. [19] effectively suppressed back radiation caused by ground plane slots by incorporating a printed mushroom-shaped EBG surface beneath the microstrip line. Similarly, the proposed design reduces back radiation by incorporating a box-shaped reflector, which is mechanically straightforward to fabricate, significantly simplifying the antenna design and manufacturing process. Ref. [20] proposed an 8×8 planar antenna array for the 60 GHz millimeter-wave band, achieving a high gain of 26.1 dBic. However, this design offered limited bandwidth improvement, and the large antenna profile restricted its application scenarios. In contrast, the proposed antenna achieves a broader bandwidth while demonstrating superior gain performance as a single antenna element.

In summary, the proposed CP-MEDA with microstrip-line aperture-coupled feeding demonstrates excellent performance as a single antenna element, achieving a broad bandwidth and high stable gain. Additionally, the antenna features a simple structure that is easy to fabricate and assemble.

5. CONCLUSION

This paper proposes a high-gain RHCP MEDA with microstrip-line aperture-coupled feeding. The RHCP characteristic is achieved by reversely extending one pair of diagonal horizontal metal plates of the traditional linearly polarized MEDA. If the other pair of diagonal horizontal metal plates is extended instead, the antenna can achieve left-hand circular polarization. The addition of a box-shaped reflector significantly enhances the antenna's gain, front-to-back ratio, and circular polarization characteristics. The measurement results show that the proposed CP antenna achieves an impedance bandwidth ($|S_{11}| < -10$ dB) of 46.8% (2.90–4.67 GHz), a 3 dB axial ratio bandwidth of 26.4% (3.58–4.67 GHz), and an overlapping bandwidth of 26.4% (3.58–4.67 GHz), with a peak measured gain of 12.9 dBic within the operating band. The antenna maintains a front-to-back ratio greater than 20 dB and a cross-polarization level less than -18 dB in the $+z$ direction within the circularly polarized frequency range, demonstrating excellent radiation performance. However, the inclusion of the box-shaped reflector increases the overall profile of the antenna, indicating the need for further optimization to reduce its size in future research. The proposed CP antenna is suitable for wireless communication base stations that require high gain and stable signal coverage.

ACKNOWLEDGEMENT

This work is supported by Tianjin Key Projects of Research and Development and Science and Technology Support in 2020 (20YFZCGX00700), and Tianjin Enterprise Science and Technology Commissioner Project in 2022 (22YDTPJC00330).

REFERENCES

[1] Muntoni, G., G. A. Casula, M. Traversari, and G. Montisci, "A wideband single-feed circularly polarized stacked patch antenna," *IEEE Access*, Vol. 12, 103 380–103 387, 2024.

[2] Hossain, A. R., M. S. I. Sagar, A. A. Mertvyy, P. K. Sekhar, and T. Karacolak, "Inkjet printed flexible dual-band dual-sense circularly polarized patch antenna," *IEEE Access*, Vol. 12, 55 424–55 433, 2024.

[3] Xia, K. and H.-F. Zhang, "Circularly polarized dielectric resonator antenna array with filtering characteristics," *Materials Research Bulletin*, Vol. 186, 113331, 2025.

[4] Wang, C., W. Hu, X. Jiang, Q. Fan, J. Huang, and H. Huang, "A wideband circularly polarized dielectric resonator antenna with flat gain response within the passband," *AEU — International Journal of Electronics and Communications*, Vol. 177, 155224, 2024.

[5] Mao, C., M. Khalily, R. Tafazolli, and A. Kishk, "Wideband dual circularly polarized helical antenna array for satellite applications," *IEEE Antennas and Wireless Propagation Letters*, Vol. 23, No. 9, 2758–2762, 2024.

[6] Cheng, Z. W., J. Deng, M. Wang, J. R. Chen, S. Wang, S. Luan, X. Liu, F. Gao, H. F. Ma, and T. J. Cui, "A compact axial-mode helical antenna based on spoof surface plasmon polaritons," *IEEE Transactions on Antennas and Propagation*, Vol. 71, No. 7, 5582–5590, 2023.

[7] Mao, C., M. Khalily, R. Tafazolli, and A. Kishk, "Wideband dual circularly polarized helical antenna with reduced mutual coupling for MIMO applications," *IEEE Transactions on Antennas and Propagation*, Vol. 72, No. 4, 3766–3771, 2024.

[8] Luk, K.-M. and H. Wong, "A new wideband unidirectional antenna element," *International Journal of Microwave and Optical Technology*, Vol. 1, No. 1, 35–44, 2006.

[9] Mak, K. M. and K. M. Luk, "A circularly polarized antenna with wide axial ratio beamwidth," *IEEE Transactions on Antennas and Propagation*, Vol. 57, No. 10, 3309–3312, 2009.

[10] Ji, X., J. Pan, Z. Du, and Q. Zhou, "A novel low-profile wideband circularly polarized magneto-electric dipole antenna," in *2021 International Conference on Microwave and Millimeter Wave Technology (ICMMT)*, 1–3, Nanjing, China, 2021.

[11] Kumar, A., A. A. Althuwayb, D. Chaturvedi, R. Kumar, and F. Ahmadfard, "Compact planar magneto-electric dipole-like circularly polarized antenna," *IET Communications*, Vol. 16, No. 20, 2448–2453, 2022.

[12] Ashouri, M. H., S. Fakhte, and M. M. Taskhiri, "A broadband high gain circularly polarized magneto-electric dipole antenna with chiral metamaterial for 5G/WIMAX wireless network," *Wireless Networks*, Vol. 30, No. 2, 845–855, 2024.

[13] Li, M., Y. Wang, C. Cai, M. Huang, Y. Wu, and Y. Qin, "Wideband dual circularly polarized multi-slot loaded magnetoelectric dipole antenna," *IEEE Antennas and Wireless Propagation Letters*, Vol. 23, No. 12, 4104–4108, 2024.

[14] Kang, K., Y. Shi, and C.-H. Liang, "A wideband circularly polarized magnetoelectric dipole antenna," *IEEE Antennas and Wireless Propagation Letters*, Vol. 16, 1647–1650, 2017.

[15] Xiao, J., J. Tian, T. Ding, C. Han, J. Wu, and Q. Ye, "A high gain circularly polarized magnetoelectric dipole antenna," in *2024 IEEE International Conference on Computational Electromagnetics (ICCEM)*, 1–2, Nanjing, China, 2024.

[16] Sun, L., A. U. Zaman, B. Yan, and W. Sheng, "Wideband high-efficiency single-layer ridge gap waveguide based circular polarized magneto-electric dipole antenna array," *IEEE Transactions on Antennas and Propagation*, Vol. 72, No. 8, 6735–6740, 2024.

[17] Xiang, L., F. Wu, C. Yu, Z. H. Jiang, Y. Yao, and W. Hong, "A wideband circularly polarized magneto-electric dipole antenna array for millimeter-wave applications," *IEEE Transactions on Antennas and Propagation*, Vol. 70, No. 5, 3876–3881, 2021.

[18] Cui, X., F. Yang, and M. Gao, "Wideband CP magnetoelectric dipole antenna with microstrip line aperture-coupled excitation," *Electronics Letters*, Vol. 54, No. 14, 863–864, 2018.

[19] Sun, J. and K.-M. Luk, "Wideband linearly-polarized and circularly-polarized aperture-coupled magneto-electric dipole antennas fed by microstrip line with electromagnetic bandgap surface," *IEEE Access*, Vol. 7, 43 084–43 091, 2019.

[20] Li, Y. and K.-M. Luk, "A 60-GHz wideband circularly polarized aperture-coupled magneto-electric dipole antenna array," *IEEE Transactions on Antennas and Propagation*, Vol. 64, No. 4, 1325–1333, 2016.

[21] Tan, Q., K. Fan, W. Yu, W. Wang, L. Liu, and G. Q. Luo, "A circularly polarized magneto-electric dipole antenna array with wide AR and impedance bandwidth for millimeter-wave applications," *IEEE Antennas and Wireless Propagation Letters*, Vol. 22, No. 9, 2250–2254, 2023.

[22] Tan, Q., K. Fan, W. Yu, Y. Yu, and G. Q. Luo, "A broadband circularly polarized planar antenna array using magneto-electric dipole element with bent strips for Ka-band applications," *IEEE Antennas and Wireless Propagation Letters*, Vol. 22, No. 1, 39–43, 2023.

[23] Li, M. and K.-M. Luk, "Wideband magneto-electric dipole antenna for 60-GHz millimeter-wave communications," *IEEE Transactions on Antennas and Propagation*, Vol. 63, No. 7, 3276–3279, 2015.

[24] Tao, J. and Q. Feng, "Dual-band magnetoelectric dipole antenna with dual-sense circularly polarized character," *IEEE Transactions on Antennas and Propagation*, Vol. 65, No. 11, 5677–5685, 2017.

[25] Xu, J., W. Hong, Z. H. Jiang, and H. Zhang, "Low-cost millimeter-wave circularly polarized planar integrated magneto-electric dipole and its arrays with low-profile feeding structures," *IEEE Antennas and Wireless Propagation Letters*, Vol. 19, No. 8, 1400–1404, 2020.